



NPM1 ablation induces HSC aging and inflammation to develop myelodysplastic syndrome exacerbated by *p53* loss

Claudia Morganti^{1,2,3,*} , Kyoko Ito^{1,2,3,†}, Chie Yanase^{1,2,3}, Amit Verma^{3,4,5}, Julie Teruya-Feldstein^{6,7} & Keisuke Ito^{1,2,3,5,**} 

Abstract

Myelodysplastic syndrome (MDS) is characterized by ineffective hematopoiesis with morphologic dysplasia and a propensity to transform into overt acute myeloid leukemia (AML). Our analysis of two cohorts of 20 MDS and 49 AML with multi-lineage dysplasia patients shows a reduction in *Nucleophosmin 1* (*NPM1*) expression in 70% and 90% of cases, respectively. A mouse model of *Npm1* conditional knockout (cKO) in hematopoietic cells reveals that *Npm1* loss causes premature aging of hematopoietic stem cells (HSCs). Mitochondrial activation in *Npm1*-deficient HSCs leads to aberrant activation of the NLRP3 inflammasome, which correlates with a developing MDS-like phenotype. *Npm1* cKO mice exhibit shortened survival times, and expansion of both the intra- and extra-medullary myeloid populations, while evoking a *p53*-dependent response. After transfer into a *p53* mutant background, the resulting *Npm1/p53* double KO mice develop fatal leukemia within 6 months. Our findings identify *NPM1* as a regulator of HSC aging and inflammation and highlight the role of *p53* in MDS progression to leukemia.

Keywords HSC aging; MDS; Nlrp3; Npm1; Tp53

Subject Categories Immunology; Signal Transduction; Stem Cells & Regenerative Medicine

DOI 10.15252/embr.202154262 | Received 2 November 2021 | Revised 28 January 2022 | Accepted 11 February 2022 | Published online 1 March 2022

EMBO Reports (2022) 23: e54262

Introduction

Myelodysplastic syndrome (MDS) refers to a heterogeneous group of closely related clonal hematopoietic disorders that are

characterized by ineffective production of blood cells and carry a high risk of transformation to acute myeloid leukemia (AML; Teferi & Vardiman, 2009). Despite extensive efforts to classify and identify the key genetic events in this pathogenesis, MDS survival rates have not dramatically improved, and most patients only survive for 4–8 months after transformation to overt leukemia (Lindsley *et al*, 2017). The pathophysiology of MDS involves multiple factors, not the least of which is aging. The incidence of MDS increases with advancing age, and the median age at diagnosis is of 65–70 years. However, whether age simply increases the probability of acquiring mutations or whether the cellular context itself contributes to pathogenesis remains an open question. The establishment of a wider range of animal models has greatly contributed to advancing our understanding of the characteristics of MDS with poor outcomes.

Nucleophosmin1 (*NPM1*) is involved in multiple cellular processes, including ribosome biogenesis and the maintenance of genomic stability (Grisendi *et al*, 2006), and is directly implicated in the development of hematopoietic malignancies. *NPM1* is the most frequently mutated gene in AML, accounting for ~60% of patients with a normal karyotype and 35% of total cases (Falini *et al*, 2005). *Npm1*^{+/-} mice exhibit increased susceptibility to leukemogenesis and have been shown to develop hematologic syndromes with features of human MDS (Grisendi *et al*, 2005; Sportoletti *et al*, 2008; Raval *et al*, 2012). *NPM1* resides on chromosome 5q35 and is lost in ~10% of MDS arising from large 5q chromosome deletion, which is observed particularly often in cases of therapy-related MDS and MDS patients with a complex karyotype (Shepherd *et al*, 1991, 1992; Nagarajan, 1995; Heinrichs *et al*, 2009; La Starza *et al*, 2010; Raval *et al*, 2012). However, the contributions of *NPM1* to hematopoiesis and MDS pathogenesis remain largely unknown, because *Npm1* is essential to embryonic development and complete

1 Ruth L. and David S. Gottesman Institute for Stem Cell and Regenerative Medicine Research, Albert Einstein College of Medicine, Bronx, NY, USA

2 Departments of Cell Biology and Stem Cell Institute, Albert Einstein College of Medicine, Bronx, NY, USA

3 Department of Medicine, Montefiore Medical Center, Albert Einstein College of Medicine, Bronx, NY, USA

4 Department of Developmental and Molecular Biology, Albert Einstein College of Medicine, Bronx, NY, USA

5 Albert Einstein Cancer Center and Diabetes Research Center, Albert Einstein College of Medicine, Bronx, NY, USA

6 Department of Pathology, Icahn School of Medicine, Mount Sinai, New York, NY, USA

7 Department of Pathology, Sloan-Kettering Institute, Memorial Sloan-Kettering Cancer Center, New York, NY, USA

*Corresponding author. Tel: +1 718 678 1278; Fax: +1 718 678 1018; E-mail: claudia.morganti@einsteinmed.edu

**Corresponding author. Tel: +1 718 678 1278; Fax: +1 718 678 1018; E-mail: keisuke.ito@einsteinmed.edu

†These authors contributed equally to this work

knockout of *Npm1* in mice leads to embryonic lethality between E11.5 and E12.5, along with both aberrant organogenesis and defective hematopoiesis (Grisendi *et al*, 2005).

To investigate NPM1's function in adult hematopoiesis, we have established conditional *Npm1* knockout mutant mice (cKO) through *Vav1Cre*-mediated inactivation of *Npm1* in hematopoietic cells. These *Npm1* cKO mice exhibit premature aging phenotype associated with mitochondrial activation in hematopoietic stem cells (HSCs) and a pro-inflammatory response. *Npm1* cKO mice exhibit shorter survival rates, myeloid population expansion, and defective HSCs. Interestingly, when transferred into a *p53* knockout background the resulting *Npm1/p53* compound mutant mice develop MDS-like hematological disorders, which transform into an aggressive and lethal form of overt leukemia in a process that mimics the progression of human MDS to leukemia.

Results

Establishment of conditional KO mice with inactivated *Npm1* in the hematopoietic system

Bone marrow (BM) samples were collected from 20 patients with MDS and 49 patients with AML with multi-lineage dysplasia (MLD, or MLD in AML) (Fig EV1A and B). *NPM1* expression levels were reduced in hematopoietic stem and progenitor cells (HSPCs) from BM of patients compared to healthy volunteers (Fig 1A). Immunohistochemical analysis showed that BM samples from patients with MDS and MLD in AML could be classified into two groups reflecting normal and low NPM1 levels (Fig 1B). ~70% of MDS and ~90% of MLD in AML patients exhibited low levels of NPM1 (Fig 1C). Notably, *NPM1* reduction was independent of Del (5q) and *NPM1c*⁺ mutations (Fig EV1C and D). These data led us to study the effect of *Npm1* loss on hematopoiesis.

To overcome the issue of embryonic lethality in *Npm1*^{-/-} mice, we first established a conditional *Npm1*-heterozygous mutant (*Npm1* cHet; *Npm1*^{F/+}*Vav1Cre*⁺) mouse model through *Vav1Cre*-mediated inactivation (Figs 1D and EV1E). The resulting *Npm1* cHet mice were then crossed with *Npm1*^{F/+}*Vav1Cre*⁻ mice to generate *Npm1*-conditional knockout (*Npm1* cKO; *Npm1*^{F/F}*Vav1Cre*⁺) mice. Although *Npm1*^{-/-} mice are known to succumb to embryonic lethality at mid-gestation owing to defective primitive hematopoiesis and severe anemia (Grisendi *et al*, 2005), these *Npm1* cKO mice were born in an expected Mendelian ratio (Fig 1E).

Since *Vav1* is expressed between E11.5–E13.5 (Chen *et al*, 2009), *Npm1*^{F/+} mice were crossed with vascular endothelial cadherin (*VEC*)-*Cre*⁺ mice to investigate whether *Npm1* is vital in earlier stages of embryonic development. *VEC* is expressed at E7.5 in the yolk sac mesoderm, at E8.5 in endothelial cells of the dorsal aorta and heart, and at E15.5 in fetal liver blood cells (Fig 1F; Chen *et al*, 2009). Breeding *Npm1*^{F/+}*VEC*-*Cre*⁻ with *Npm1*^{F/+}*VEC*-*Cre*⁺ mice revealed that *Npm1*^{F/F}*VEC*-*Cre*⁺ mice had a disadvantage in birth rate and were not born in the expected Mendelian ratio (Fig 1G). These data confirmed that *Npm1* plays a crucial role in development at the earliest stages and that the loss of *Npm1* at E7.5 and particularly at E11.5 is compatible with life, allowing us to obtain an *in vivo* model for the study of *Npm1* loss in adult hematopoiesis.

Npm1 loss leads to an aging phenotype and activation of mitochondria in HSCs

Myelodysplastic syndrome occurs primarily in elderly patients, and hematopoietic aging itself is a key factor in the pathophysiology of the disease. We observed a decrease in *Npm1* expression levels in the bone marrow mononuclear cells (BM-MNCs) of young versus old wild-type mice (Fig 2A).

When compared to those from healthy young individuals, HSCs from both aged healthy individuals and MDS patients show similar phenotypes, including levels of HSC expansion, myeloid-biased HSCs, and decreased erythroid output (Morrison *et al*, 1996; Chambers *et al*, 2007; Pang *et al*, 2013). 4-months-old *Npm1* cKO mice showed increased frequency of phenotypic HSCs (c-Kit⁺Sca-1⁺Lin⁻ (KSL) CD135⁻CD48⁻CD150⁺), which was also observed in 15-months-old *Npm1* cHet and in 2-years-old wild-type (WT) mice (Figs 2B and EV2A). The increase in phenotypic HSCs in *Npm1* cKO mice at 4 months was associated with decrease in cytoskeletal polarity in HSCs, as detected by tubulin and CDC42 localization (Fig 2C and D), a well-known marker of HSC aging (Florian *et al*, 2012). *In vitro* colony-replating assays revealed functional loss in *Npm1* cKO HSCs (Fig 2E). *Npm1* cKO HSCs showed the same phenotype as aged HSCs derived from 18/24-months-old mice (Fig 2B–E). Notably, at the age of 15 months, HSCs from *Npm1* cHet mice also showed reduced *in vitro* colony-replating ability (Fig EV2B).

Since several studies proposed that mitochondria play a critical role in aging process (Ito *et al*, 2006; Mohrin *et al*, 2015), we investigated the mitochondria morphology and physiology in *Npm1* cKO HSCs. Immunofluorescent analysis of mitochondrial features showed overall aberrant mitochondrial activation in *Npm1*-deleted HSCs, with increases in mitochondrial volume and number (Fig 2F), mitochondrial membrane potential (Fig 2G), and mitochondrial reactive oxygen species (ROS) production (Fig 2H). Interestingly, mitochondrial volume increased in KSL cells, but not in more committed Lin⁻ cells (Fig EV2C), while no differences were detected in mitochondrial membrane potential (Fig EV2D) or mitochondrial ROS production (Fig EV2E) in either KSL and Lin⁻ cells. Analysis of HSCs derived from 18/24-months-old mice confirmed that increased mitochondrial volume was linked to the aging process (Fig 2F).

We then used a human MDS cell line model (MDS-L cells) to test whether reduced NPM1 levels affect mitochondrial physiology in human hematopoiesis. MDS-L cells were derived from the bone marrow of an MDS patient with deletion of the 5q chromosome [del (5q)] (Tohyama *et al*, 1994; Matsuoka *et al*, 2010; Kida *et al*, 2018). We optimized the transfection of MDS-L cells with siNPM1 so that a nearly complete reduction of NPM1 levels was obtained (Fig 2I). We have confirmed that, as in the mitochondrial phenotypes found in *Npm1*-deleted murine HSCs (Fig 2F–H), mitochondrial volume and number (Fig 2J), mitochondrial membrane potential (Fig 2K), and mitochondrial ROS production (Fig 2L) were all increased in human MDS-L cells treated with siNPM1.

Collectively, these data suggest that NPM1 loss triggers aberrant activation of mitochondria in HSCs which is linked to aging-like phenotypes. The premature aging phenotypes observed in *Npm1* cKO mice inspired us to use this *in vivo* model to further explore the contribution of aging to MDS progression.

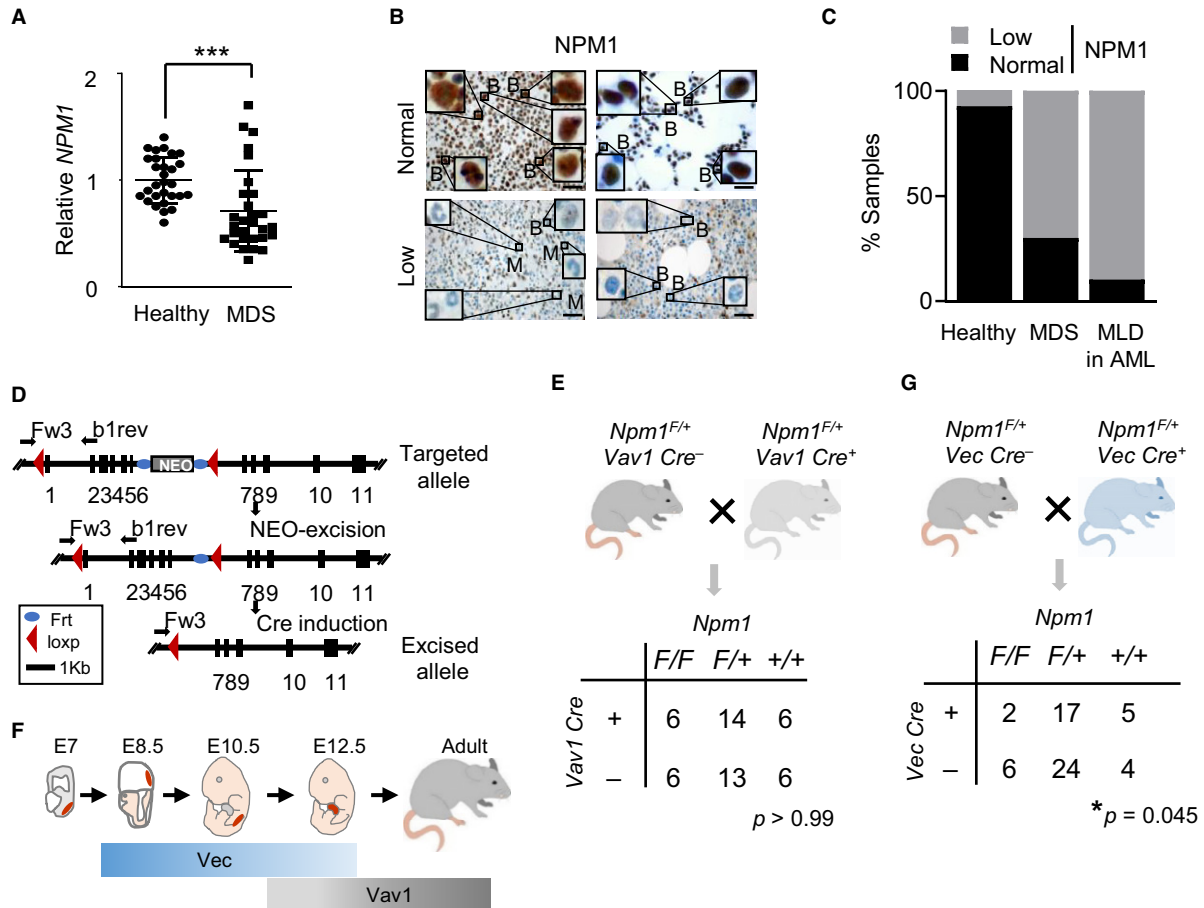


Figure 1. *Npm1* conditional mutants in the hematopoietic system.

- A *NPM1* expression in CD34⁺Lin⁻ cells from myelodysplastic syndrome (MDS) patients compared to healthy volunteers ($n = 29$). Data are shown as mean \pm SD. Unpaired two-tailed t-test, *** $p < 0.001$.
- B Representative staining of NPM1 protein levels in bone marrow samples of MDS or acute myeloid leukemia with multi-lineage dysplasia (MLD in AML). Insets show representative staining in blasts [B] and in differentiated myeloid cells [e.g., neutrophil, M] with a high magnification. Scale bar, 50 μ m.
- C Percentages of patient samples with NPM1-low and NPM1-normal in healthy, MDS and MLD in AML groups.
- D Schematic strategy of *Npm1* conditional knockout. Excision of exons 1–6 from the *Npm1* allele by Cre-recombinase produces an *Npm1*-knockout allele. Hypomorphic allele (top), NEO-free allele (middle, Flox) and excised allele are shown. The genomic sequence is depicted as a black line, with black boxes representing exons 1–11. Grey box, red triangles and arrows represent an Frt (blue)-flanked neomycin resistance cassette (NEO), the loxP site, and genotyping primers, respectively.
- E Schema of mating strategy and numbers of viable pups at weaning bearing the 6 possible genotypes for *Vav1-Cre*. A Chi-square test determined any difference between observed proportions and expected proportions.
- F Schematic representation of *Vec* and *Vav1* expression during embryogenesis.
- G Schema of mating strategy and numbers of viable pups at weaning bearing the 6 possible genotypes for *Vec-Cre*. A Chi-square test determined any difference between observed proportions and expected proportions.

Enhanced pro-inflammatory signaling contributes to aberrant myeloid expansion in *Npm1* cKO mice

Mitochondrial stress has recently been shown to promote aberrant activation of the NLRP3 (NOD-, LRR- and pyrin domain-containing protein 3) inflammasome, which subsequently triggers functional decline of HSCs during aging (Luo *et al.*, 2019). We have observed increases of ~40% in *Nlpr3* expression in BM-MNCs from *Npm1* cKO mice compared to littermate control mice (Fig 3A). Assembly of the NLRP3 inflammasome leads to caspase-1-dependent release of pro-inflammatory cytokines such as IL-1 β (Swanson *et al.*, 2019). To verify the inflammation status of the *Npm1* cKO mice, serum samples

from the *Npm1* cKO and control mice were assessed against a panel of 13 cytokines produced by innate immune cells. We found an overall pro-inflammatory trend in *Npm1* cKO mice, with significant increases in levels of IL-1 β , IL-6, IFN γ , and IL-27 (Figs 3B and EV3A).

IL-1 accelerates the myeloid-bias differentiation process (Pietras *et al.*, 2016) that is typical of MDS patients. Bone marrow analysis of *Npm1* cKO mice revealed increased myeloid production, particularly of CD11b⁺Gr1^{mid} cells, which previous reports have associated with oncogenic phenotypes¹⁷ (Fig 3C). Although no significant differences were detected in the amount of myeloid progenitor-enriched cells (c-Kit⁺Sca-1⁻Lin⁻) and common myeloid progenitor (Lin⁻Sca-1⁻c-Kit⁺CD16/32^{low}CD34⁺, or CMP), the megakaryocyte-erythroid progenitor

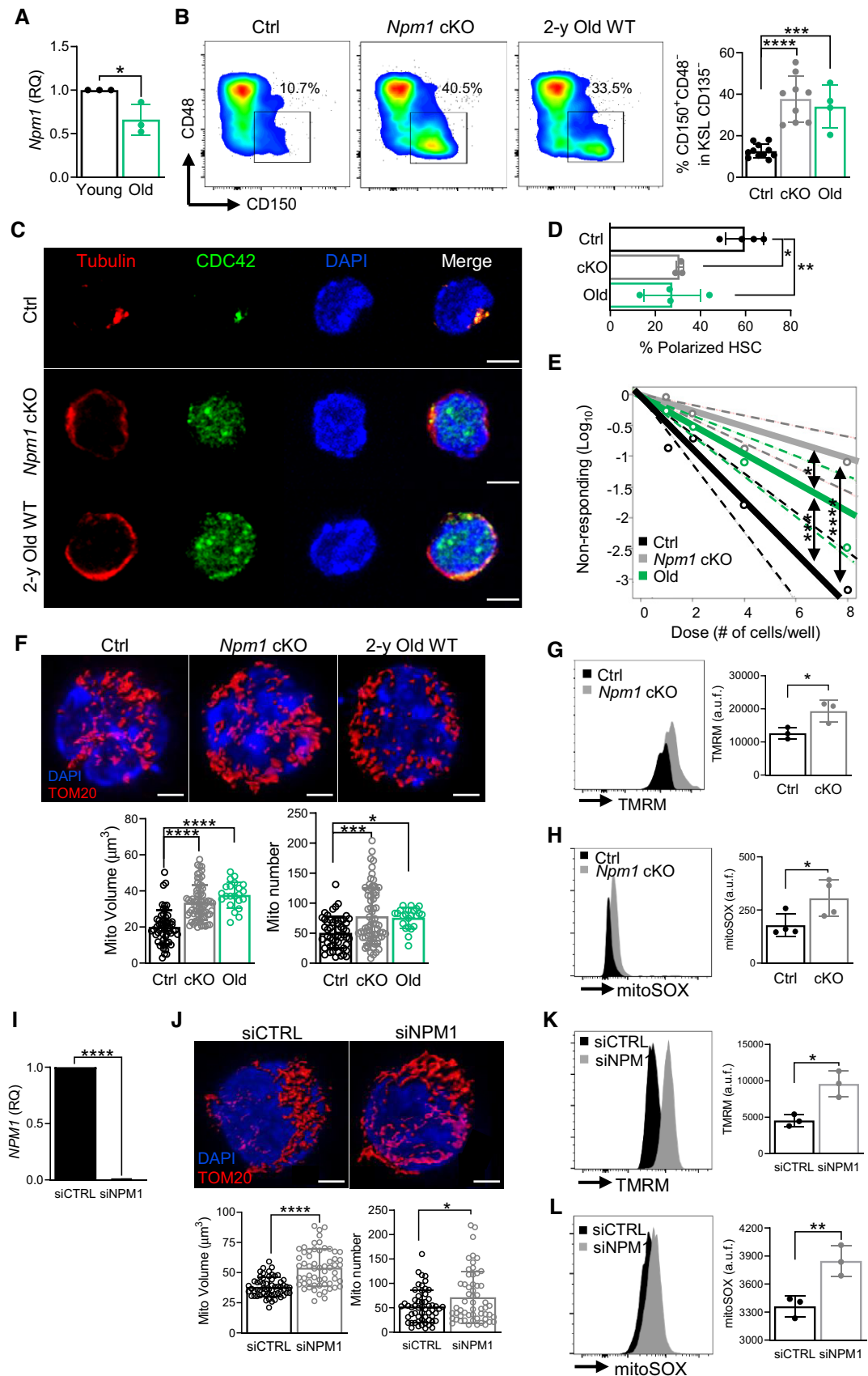


Figure 2.

Figure 2. *Npm1* loss causes an HSC aging phenotype.

- A *Npm1* expression levels (relative quantitation, RQ) in BM-MNCs of young (3–6 months old) and old (12–18 months old) wild type (WT) mice ($n = 3$ mice per group).
- B Representative flow cytometry analysis of phenotypic HSCs [$c\text{-Kit}^+ \text{Sca-1}^- \text{Lin}^-$ (KSL) $\text{CD135}^- \text{CD48}^- \text{CD150}^+$] in the bone marrow of 4-months-old Ctrl ($Npm1^{F/F} \text{Vav1Cre}^-$), 4-months old *Npm1* cKO ($Npm1^{F/F} \text{Vav1Cre}^+$) and 2-years Old WT mice (left). Mean percentages of the indicated fraction are shown (right, $n = 4$ –9 mice per group).
- C Representative distribution of Tubulin and CDC42 in Ctrl, 4-months old *Npm1* cKO and 2-years old WT HSCs determined by IF. Scale bars, 5 μm .
- D Quantification of percentage of cytoskeletal polarized HSCs ($n = 79$ cells in Ctrl, $n = 120$ cells in cKO, $n = 82$ cells in Old, from 4 Ctrl and Old mice and 3 cKO mice).
- E *In vitro* colony replating ability of HSCs from Ctrl, 4-months old *Npm1* cKO and 2-years old WT mice determined by limiting-dilution assay. Overall test for differences in stem cell frequencies between any of the groups calculated by chi-square test, * $P < 0.05$, *** $P < 0.001$, **** $P < 0.0001$. The slope of the line is the log-active cell fraction. The dashed lines give the 95% confidence interval.
- F HSCs of Ctrl, 4-months old *Npm1* cKO and 2-years old WT mice were sorted and stained for TOM20. Representative images (top) and quantification of mitochondrial volume and number (bottom) in single cells ($n = 58$ cells in Ctrl, $n = 70$ cells in cKO and $n = 23$ cells in Old, from 3 mice per group), identified by volume rendering of TOM20. Scale bars, 2 μm .
- G Representative flow cytometry histogram (left) and quantification of TMRM median intensity (right, $n = 3$ mice per group) in HSCs from the indicated genotyped mice.
- H Representative flow cytometry histogram (left) and quantification of mitoSox median intensity (right, $n = 4$ mice per group) in HSC fraction.
- I *NPM1* expression levels (relative quantitation, RQ) in MDS-L cells transfected with *siNPM1* or control (*siCTRL*) ($n = 3$ transfected MDS-L cultures).
- J Representative images (top) and quantification of mitochondrial volume and number (bottom), identified by volume rendering of TOM20, in MDS-L cells transfected with *siNPM1* or control (*siCTRL*) ($n = 58$ cells per group, from 3 transfected MDS-L cultures). Scale bars, 2 μm .
- K Representative flow cytometry histogram (left) and quantification (right, $n = 3$ transfected MDS-L cultures) of TMRM median intensity in MDS-L cells transfected with *siNPM1* or control.
- L Representative flow cytometry histogram (left) and quantification (right, $n = 3$ transfected MDS-L cultures) of mitoSox median intensity in MDS-L cells transfected with *siNPM1* or control.
- Data information: All data are shown as mean \pm SD. Panels A, and G–L, Unpaired two-tailed *t*-test; panels B, D and F, ANOVA test, compare to Ctrl, * $P < 0.05$, ** $P < 0.01$, *** $P < 0.001$, **** $P < 0.0001$.

($\text{Lin}^- \text{Sca-1}^- \text{c-Kit}^+ \text{CD16/32}^{\text{low/neg}} \text{CD34}^{\text{low/neg}}$, or MEP) cells decreased, while the granulocyte-macrophage progenitors ($\text{Lin}^- \text{Sca-1}^- \text{c-Kit}^+ \text{CD16/32}^{\text{high}} \text{CD34}^+$, or GMP) cells increased in *Npm1* cKO mice, leading to a biased differentiation process (Figs 3D and EV3B). Likewise, the number of hematopoietic stem and progenitor cells (HSPCs) ($\text{c-Kit}^+ \text{Sca-1}^- \text{Lin}^-$ fraction, or KSL) was not drastically affected (Fig EV3B), but these cells' ability to form M-colonies *in vitro* was substantially increased compared to controls (Fig 3E).

Peripheral blood (PB) smears revealed the appearance of anisocytosis, dysplastic myeloid cells, dysplastic erythroid cells, dysplastic monocytes, and dysplastic neutrophils in 4-months old *Npm1* cKO mice (Fig 3F). Although the myeloid population increased only slightly in the spleen (Fig EV3C), *Npm1* cKO mice clearly exhibited splenomegaly (Fig 3G) with a significant increment in *c-Kit* positivity in the myeloid fraction (Fig 3H).

All these data suggest an alteration of physiological hematopoiesis, characterized by unbalanced differentiation, which shares features with MDS.

***p53* deletion in DKO mice triggers blast accumulation and leukemic transformation**

Npm1 cKO mice exhibited a median survival of 353 days, while the loss of only one allele of *Npm1* ($Npm1^{F/+} \text{Vav1Cre}^+$, or *cHet*) was associated with life expectancy of ~ 1.5 years, suggesting that the homozygous deletion of *Npm1* in the hematopoietic system leads to a more aggressive and/or rapid hematological malignancy (Fig 4A). A hypocellular marrow was observed in *Npm1* cKO mice as early as 4 months of age, which subsequently declined toward fatal bone marrow failure (Figs 4B and EV4A).

Figure 3. Inflammation and myeloid expansion in *Npm1* cKO mice.

- A Levels of *Nlrp3* expression (relative quantitation, RQ) in Ctrl ($Npm1^{F/F} \text{Vav1Cre}^-$) and cKO ($Npm1^{F/F} \text{Vav1Cre}^+$) mice (4-months old, $n = 4$ mice per group).
- B Quantification of IL-1 β , IL-6, IFN γ , and IL-27 inflammatory cytokines in serum from Ctrl and cKO mice (4-months old, $n = 8$ –10 mice per group).
- C Representative flow plot (top) and quantification (bottom) of myeloid fractions ($\text{CD11b}^+ \text{Gr1}^+$) and myeloid fraction subpopulation related to malignancy ($\text{CD11b}^+ \text{Gr1}^{\text{mid}}$) in the bone marrow of Ctrl and cKO mice ($n = 5$ –8 mice per group).
- D Representative flow plot (top) and quantification (bottom) of myeloid progenitors: common myeloid progenitor (CMP), $\text{Lin}^- \text{Sca-1}^- \text{c-Kit}^+ \text{CD16/32}^{\text{low}} \text{CD34}^+$; granulocyte-macrophage progenitor (GMP), $\text{Lin}^- \text{Sca-1}^- \text{c-Kit}^+ \text{CD16/32}^{\text{high}} \text{CD34}^+$; megakaryocyte-erythroid progenitor (MEP), $\text{Lin}^- \text{Sca-1}^- \text{c-Kit}^+ \text{CD16/32}^{\text{low/neg}} \text{CD34}^{\text{low/neg}}$ in the bone marrow of Ctrl and cKO mice ($n = 4$ mice per group).
- E *In vitro* colony-forming capacity of progenitor cells. Sorted KSL cells were cultured in semisolid medium. Counting and classification of colonies were performed in independent littermate pairs ($n = 3$ mice per group). GEMM, Colony-forming unit-granulocyte, erythroid, macrophage, and megakaryocyte; GM, Colony-forming unit-granulocyte and macrophage; M, Colony-forming unit-macrophage; E, Burst-forming unit-erythroid.
- F Representative peripheral blood (PB) smears. Insets show the differentiated granulocytes (a, b) in control mice, and anisocytosis (c), dysplastic myeloid cells (d–g) in *Npm1* cKO mice ($Npm1^{F/F} \text{Vav1Cre}^+$). *Npm1* cKO mice show dysplastic erythroid cells (polychromatophilic, blue arrowhead; schistocyte, blue-outlined arrowhead; tear drop, Howell-jolly bodies, black arrowhead; black-outlined arrowhead), dysplastic monocytes (black arrow), and dysplastic neutrophils (d–f). Scale bars, 10 μm .
- G Representative pictures (right) and weights (left, $n = 6$ –8 mice per group) of spleens of 4-months old Ctrl and *Npm1* cKO mice.
- H *c-Kit* positivity in myeloid fraction in the spleen ($n = 5$ mice per group).
- Data information: All data are shown as mean \pm SD. Unpaired two-tailed *t*-test, ns $P > 0.05$, * $P < 0.05$, ** $P < 0.01$, *** $P < 0.001$.

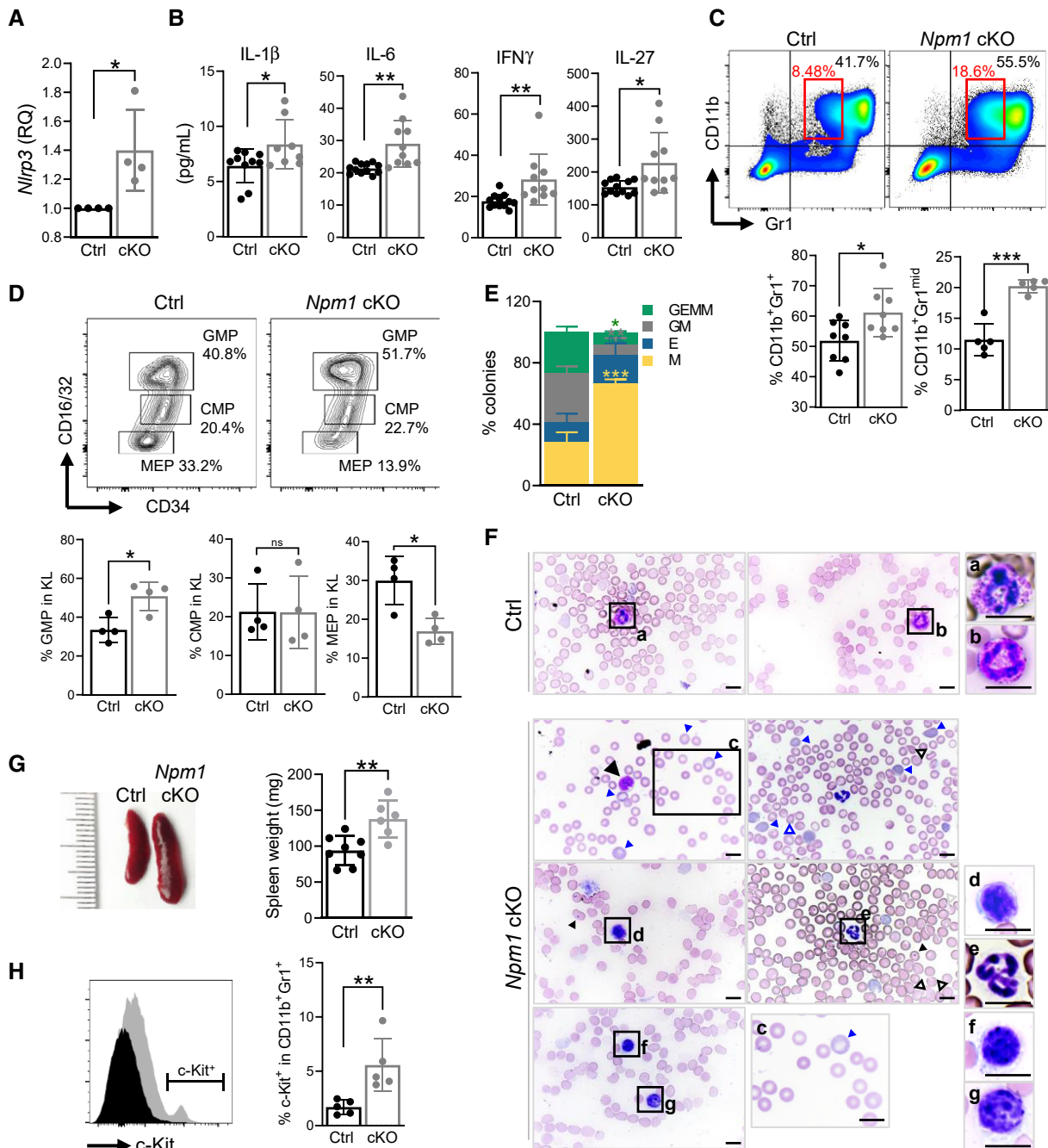


Figure 3.

As previously reported (Grisendi *et al*, 2006), *Npm1* loss evokes a p53 response. When *Npm1* is lost, levels of p53 protein and its downstream target, *p21*, both increased (Fig 4C and D). We confirmed that levels of *p53* and *p21* similarly increased in human MDS-L cells treated with siNPM1 for 48 h (Fig EV4B and C). To better understand the link between *Npm1* and p53, we have established *Npm1/p53* compound mutant (Double Knockout or DKO; *Npm1^{F/F}p53^{-/-}Vav1Cre⁺*) mice. All possible genotyped mice were born in expected Mendelian ratio (Fig EV4D), grew normally until weaning, and were followed until natural death (Figs 4A and EV4E). As expected, *p53*

loss (*p53* KO) caused shorter survival rates, with mice dying within 1 year, while Double Het (*Npm1^{F/+}p53^{+/-}Vav1Cre⁺*) mice exhibited survival rates similar to *Npm1* cKO mice. Interestingly, as early as 2–3 months of age, DKO mice began to display signs of distress such as lethargy and ruffling of fur, and most of them died within 6 months (Median survival: 110 days) (Fig 4A). Notably, the majority (> 90%) of DKO mice died of myeloid, but not lymphoid, leukemia.

At 2 months of age, DKO mice were already exhibiting increased WBC counts with moderate anemia and lower platelet counts in the PB (Figs 4E left and EV4F). Flow cytometry analysis revealed an enhanced

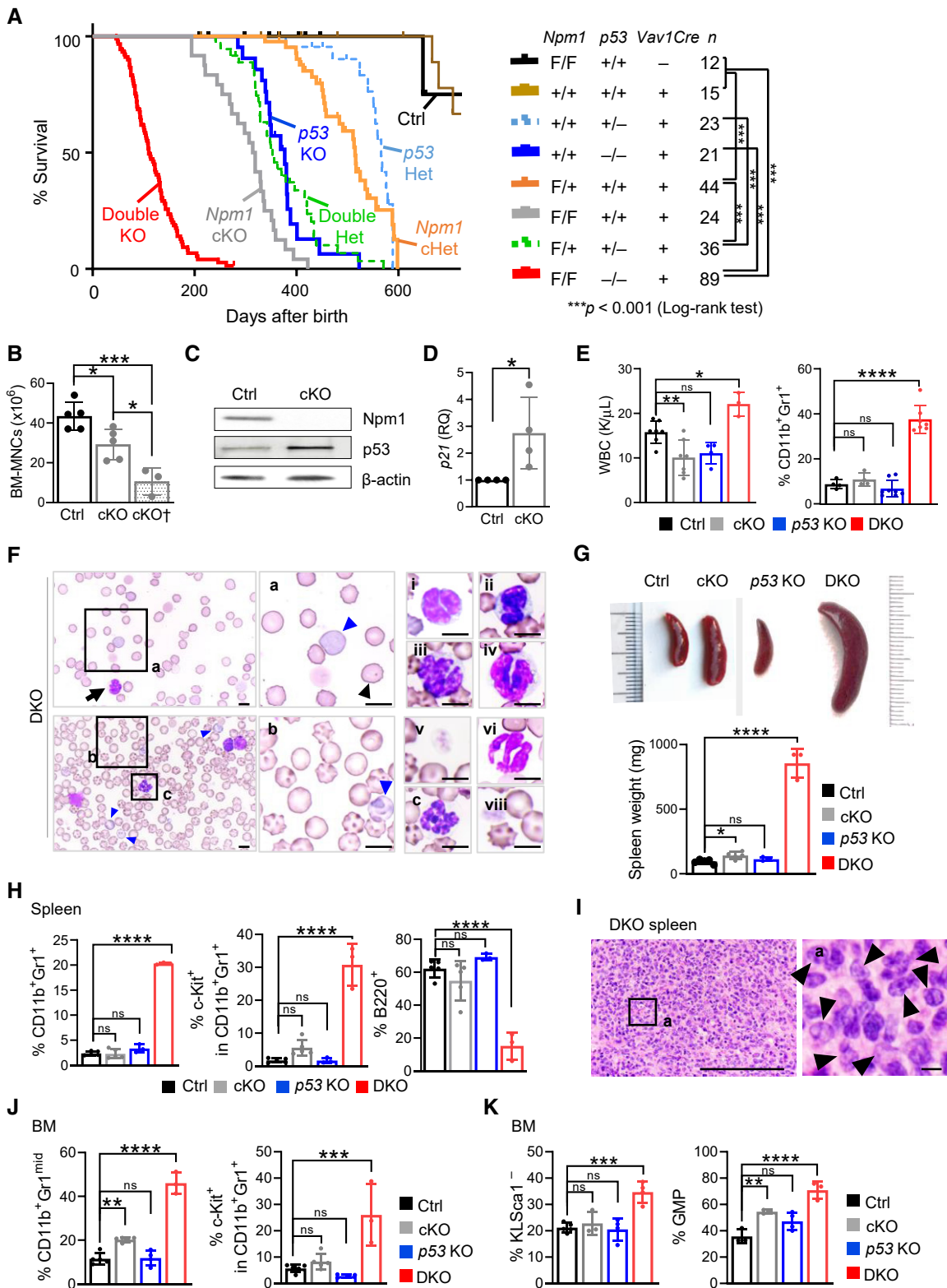


Figure 4.

biased myeloproliferative phenotypes in the PB of DKO mice; the positivity for CD11b and Gr1 was drastically increased (Figs 4E right and EV4G), while B220 positivity was reduced (Fig EV4H).

PB smear specimens showed that 2-months old DKO mice suffered from multi-lineage dysplastic features found in human MDS (Goasguen & Bennett, 1992; Komrokji *et al*, 2010; Wang, 2011;

Figure 4. *Npm1/p53* double KO mice develop a myeloid dysplastic syndrome-like disease.

- A Survival curves of Ctrl ($Npm1^{F/F}Vau1Cre^{-}$), cKO ($Npm1^{F/F}Vau1Cre^{+}$), p53 KO ($Npm1^{F/F}p53^{-/-}Vau1Cre^{-}$) and DKO ($Npm1^{F/F}p53^{-/-}Vau1Cre^{+}$) mice. Overall survival of the indicated mice was examined by plotting Kaplan-Meier survival curves. Log-rank test was used to generate *P* values, ****P* < 0.001.
- B Amount of total bone marrow mononuclear cells (BM-MNCs) in Ctrl, 4-months old *Npm1* cKO mice and moribund *Npm1* cKO (cKO[†]) (*n* = 3–5 mice per group).
- C *Npm1* and p53 protein levels in KSL cells of Ctrl ($Npm1^{F/F}Vau1Cre^{-}$), and cKO ($Npm1^{F/F}Vau1Cre^{+}$) mice.
- D *p21* expression levels in BM-MNCs of Ctrl and *Npm1* cKO mice (4-months old, *n* = 4 mice per group).
- E White blood cell (WBC) count (left) and myeloid fraction (CD11b⁺Gr-1⁺, right) in PB (*n* = 3–8 mice per group).
- F Representative PB smears of DKO mice. Insets show anisocytosis (a), poikilocytosis (b) and dysplastic myeloid cell (c). DKO mice show dysplastic erythroid cells (polychromatophilic, blue arrowhead), Howell-Jolly bodies, (black arrowhead in insert a), dysplastic monocytes (black arrow, and i–v), dysplastic neutrophils (vi), a pseudo-Pelger-Huet anomaly (ii), and dysplastic platelets (giant platelet, iv and vii). Scale bars, 10 μm.
- G Pictures of spleens (top) and spleen weight quantification (bottom, *n* = 3–5).
- H Percentages of myeloid fraction (CD11b⁺Gr1⁺), c-Kit positivity, and B220 positivity in spleen samples (*n* = 3–5).
- I Representative H&E staining of sections of the spleen of 2-months old DKO mice with myeloid disorders. Arrowheads (right) indicate the infiltrating myeloid blasts. Scale bars, 250 μm (left) and 10 μm (right), respectively.
- J Myeloid subtype (CD11b⁺Gr1^{mid}), and c-Kit positivity inside myeloid fraction in BM (*n* = 3–5).
- K c-Kit⁺Sca1⁻Lin⁻ (KL Sca1⁻) and granulocyte-macrophage progenitor (GMP) in the BM (*n* = 3–4).

Data information: All data are shown as mean ± SD. Panel D, unpaired two-tailed *t*-test; Panels B, E, G, H, J, K, ANOVA test, compare to Ctrl, ns *P* > 0.05, **P* < 0.05, ***P* < 0.01, ****P* < 0.001, *****P* < 0.0001.

Giagounidis & Haase, 2013). Dysplasia in monocytic lineages were predominant, and blast infiltration (Fig 4F, insert c) begun in the PB. Defective erythroid maturation (i.e., Howell-Jolly bodies, anisocytosis, polychromasia, and poikilocytosis), and dysplastic platelets (i.e., giant platelets) and neutrophils were also noted (Fig 4F).

DKO mice exhibited a 6-fold increase in splenomegaly on average compared to their littermate controls (Fig 4G). This change in spleen size was attributed to myeloid infiltration, with an increase in CD11b positivity, increase in c-Kit positivity in the myeloid fraction, and a decrease in B220 positivity (Figs 4H and EV5A), as well as a disruption in the splenic architecture and infiltration of myeloid blasts (Fig 4I).

We next assessed the BM in order to characterize further the hematological disorders in *Npm1/p53* compound mutant mice. Much as in the PB, the monocyte-enriched fraction increased, particularly the CD11b⁺Gr1^{mid} myeloid cell subset (Figs 4J left and EV5B), which was associated with c-Kit positivity (Fig 4J right). The skewed myeloid/lymphoid ratio observed in compound mutants was also found at the progenitor stage: the myeloid progenitor-enriched fractions (c-Kit⁺Sca1⁻Lin⁻ cells) increased (Fig 4K left), while the lymphoid progenitors (Lin⁻CD127⁺c-Kit^{mid}Sca1⁺, common lymphoid progenitor, or CLP) decreased (Fig EV5C). CMP cells slightly decreased, while in DKO mice, GMP cells increased at the expense of MEP cells (Figs 4K right and EV5D). CFU assays were conducted to assess the potential for proliferation and hematopoietic differentiation. HSPCs from DKO mice exhibited enhanced colony-forming capacity (~1.5 times), with the ratio of macrophage colonies increasing while the differentiation capacity toward the erythroid lineage was impaired (Fig EV5E and F).

The malignant nature of myeloid expanding cells was assessed by *in vivo* transplantation assays. BM-MNCs from controls, *Npm1* cKO, *p53* KO, and DKO mice were transplanted into irradiated recipient mice with competitor BM-MNCs (Fig 5A). The myeloid malignancies in *Npm1/p53* compound mutants were readily transplantable, with all recipient mice transplanted with DKO donor marrow cells initiating lethal forms of myeloid disorders within one month (Fig 5B). On the other hand, recipient mice transplanted with *Npm1* cKO donor marrow cells died after 8–12 weeks, with a significant higher survival rate than those transplanted with DKO donor

cells (Fig 5B). The hematological phenotypes in recipient mice were similar to those observed in older primary *Npm1* and *Npm1/p53* compound mutant mice (e.g., 4–6 months old), since reconstitution stress further accelerated disease progression. The BM analysis of lethargic/dead recipient mice with *Npm1* cKO donor showed BM failure, characterized by the drastic decrease of BM-MNCs due to the expansion of progenitor cells (c-Kit⁺Sca1⁻Lin⁻) and the decrease in KSL and HSC pools (Fig 5C and D). After DKO donor transplantation, monocyte-enriched CD11b⁺Gr1^{mid} cells drastically increased in recipient mice and were associated with dysplasia and myeloid blasts (Fig 5E and F), suggesting leukemic transformation.

The escape from p53-dependent pathways protects from bone marrow failure, but leads to exacerbation of MDS

Our two mouse models showed different paths of disease progression: bone marrow failure and AML transformation in *Npm1* cKO and DKO, respectively. We subsequently analyzed several aspects of these models to elucidate the mechanisms of their divergent progression.

No differences were detected between *Npm1* cKO and DKO in HSC fraction expansion (Fig 6A), mitochondria volume (Fig 6B) or cytoskeletal polarization (Fig 6C), suggesting that *Npm1* loss causes the aging phenotype in a p53-independent way.

Although hematopoiesis in *p53* het or KO mice appears to proceed normally (Lotem & Sachs, 1993), numerous studies have identified key roles for p53 in the proliferation, differentiation, and apoptosis of hematopoietic cells (Asai *et al.*, 2011). The upregulation of p53 in *Npm1* cKO mice triggered entrance into the senescence phase, marked by activation of β-galactosidase enzymes (Fig 6D) and an increase in apoptotic cell numbers, as detected by Annexin V staining (Fig 6E). These impairments in senescence and apoptosis processes were not found in the DKO mice and may explain the peculiar hypocellularity in the marrow observed in *Npm1* cKO mice as early as 4 months of age, which subsequently declines toward fatal bone marrow failure (Fig 4C).

DKO mice showed an overall increasing trend in inflammation. *Nlrp3* expression was significantly upregulated (Fig 6F) and IL-1β production drastically increased in the serum of DKO mice

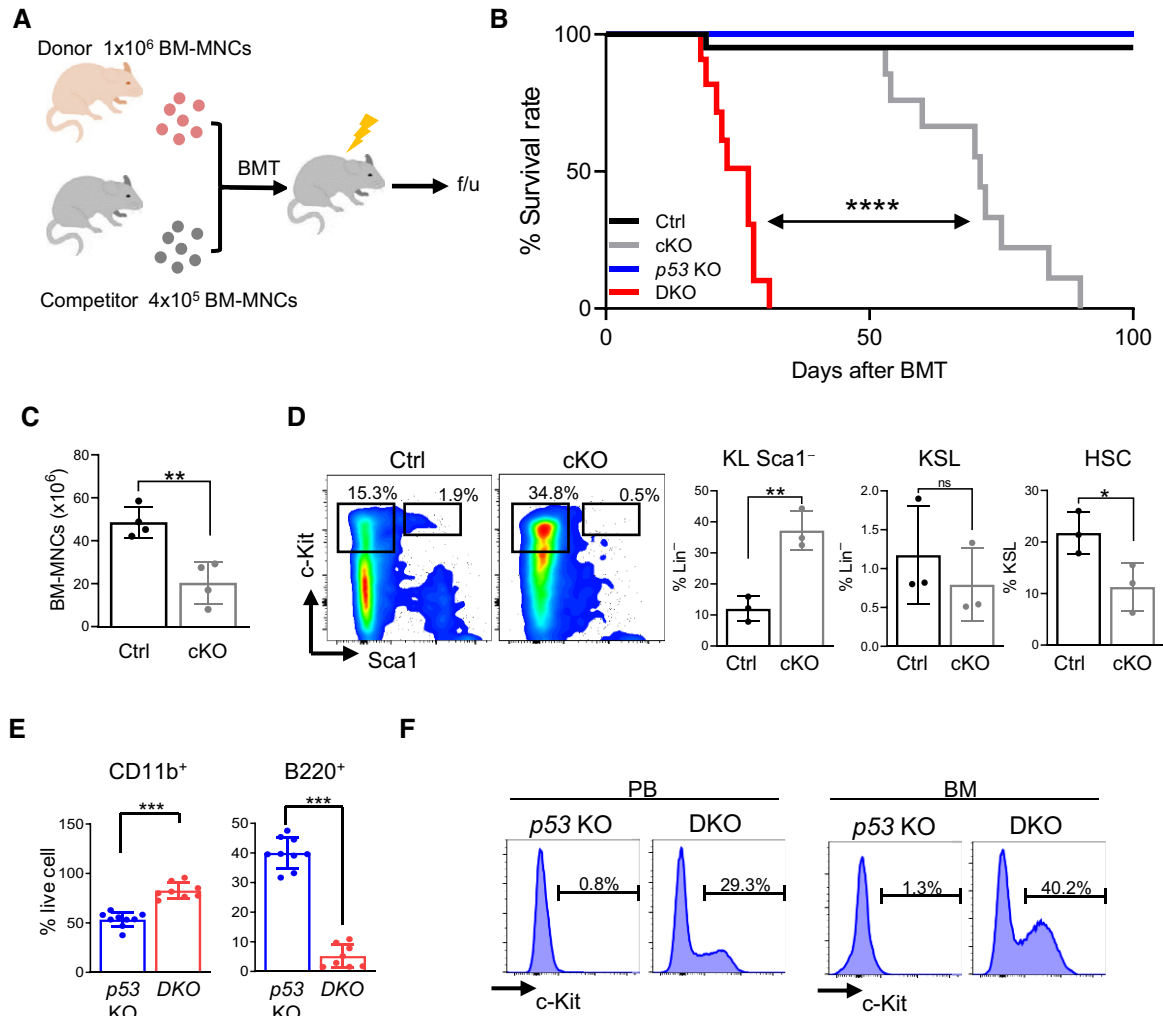


Figure 5. In vivo transplatability of the disease.

A 1.0×10^6 bone marrow mononuclear cells (BM-MNCs) from controls ($Npm1^{F/F}Vau1Cre^{-}$), $Npm1$ cKO ($Npm1^{F/F}Vau1Cre^{+}$), $p53$ KO ($Npm1^{F/F}p53^{-/-}Vau1Cre^{-}$) and DKO ($Npm1^{F/F}p53^{-/-}Vau1Cre^{+}$) mice were transplanted into irradiated recipient mice with 4.0×10^5 competitor (C57/BL6 Ly5.1) BM-MNCs.
B Survival curves of recipient mice are shown ($n = 9-10$ mice per group). Log-rank test was used to generate P values, **** $P < 0.0001$.
C Quantification of total BM-MNCs in Ctrl mice and lethargic/dead $Npm1$ cKO mice ($n = 4$ mice per group).
D Representative flow cytometry analysis and quantification of KL Sca1⁻, KSL cells and HSCs (KSL CD150⁺CD48⁻) in lethargic/dead $Npm1$ cKO mice ($n = 3$ mice per group).
E, F Percentages of CD11b⁺ and B220⁺ in PB (E), and c-Kit positivity in myeloid fraction in PB (F left) and BM (F right) of $p53$ KO and lethargic/dead DKO mice ($n = 8-9$ mice per group).

Data information: All data are shown as mean \pm SD. Unpaired two-tailed t-test, ns $P > 0.05$, * $P < 0.05$, ** $P < 0.01$, *** $P < 0.001$, **** $P < 0.0001$.

(Fig 6G). Interestingly, we observed increased levels of new cytokines, such as IL-23 (Fig 6H). This led us to hypothesize that different inflammatory pathways could be recruited in the DKO model.

Finally, p53 status was analyzed in both the MDS and AML patient' cohorts. Wild-type TP53 protein is normally undetectable by immunohistochemistry (IHC) due to its short half-life, and therefore, as expected, TP53 was undetectable or rarely detectable in samples from either healthy volunteers or a significant portion of MDS patients. In contrast, as mutated TP53 can accumulate within the nucleus due to its prolonged half-life, the detection of TP53 protein by IHC suggests that an underlying mutation is present in

the TP53 gene. This has proved to be the case in specific subsets of MDS samples, and we have confirmed that $> 70\%$ of AML patients with MLD exhibit altered levels of TP53 (Fig 6I). Collectively, the data regarding the status of NPM1 and TP53 show that, while 70% of MDS patients exhibit only low NPM1 expression, abnormal TP53 expression is frequently observed during disease progression toward overt leukemia.

Collectively, our data suggest that p53 serves as a guardian during stress conditions, and the inactivation of *Npm1* leads to enhanced p53 levels and apoptosis, which prevent further deterioration in hematopoiesis and leukemia development, but lead to bone marrow failure.

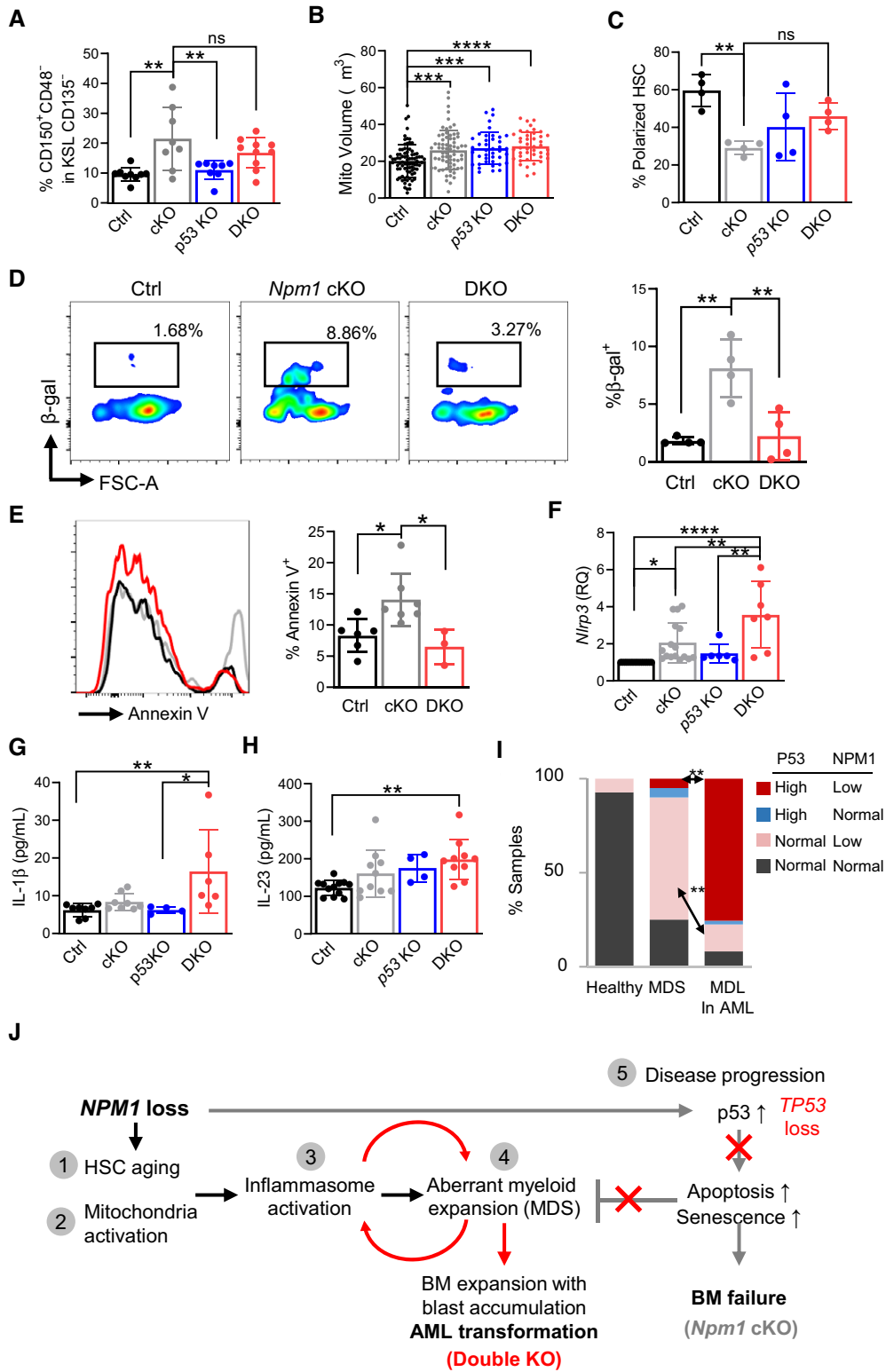


Figure 6.

Discussion

NPM1 deregulation is a common event in various malignancies (Lopez *et al*, 2020), and *NPM1* frame-shift mutations, known as

NPM1^c to indicate the cytoplasmic localization of NPM1, are found in one third of AML patients (Falini *et al*, 2005; Naoe *et al*, 2006). Although *NPM1*^c expression is always heterozygous, NPM1 forms heterodimers with wild-type NPM1 in a dominant-negative manner,

Figure 6. Escape from p53 dependent pathway triggered by *Npm1* loss leads to exacerbation of MDS.

- A Mean percentages of phenotypic HSCs [c-Kit⁺Sca-1⁺Lin⁻ (KSL) CD135⁻CD48⁻CD150⁺] in the bone marrow (BM) of 4-months old controls (*Npm1^{F/F}Vav1Cre⁻*), *Npm1* cKO (*Npm1^{F/F}Vav1Cre⁺*), *p53* KO (*Npm1^{F/F}p53^{-/-}Vav1Cre⁻*) and DKO (*Npm1^{F/F}p53^{-/-}Vav1Cre⁺*), (*n* = 8 mice per group).
- B Quantification of mitochondrial volume, identified by volume rendering of TOM20, in sorted HSC (*n* = 83 cells in Ctrl, *n* = 70 cells in cKO, *n* = 41 cells in *p53* KO and *n* = 43 cells in DKO, from 3 mice per group).
- C Percentage of cytoskeletal polarized HSCs (*n* = 47 cells in Ctrl, *n* = 46 cells in cKO, *n* = 30 cells in *p53* KO and *n* = 102 cells in DKO, from 4 mice per group).
- D Representative flow plot (left) and quantification (right) of β -galactosidase enzyme activity (β -gal) staining in KSL fraction (*n* = 4 mice per group).
- E Representative flow histograms (left) and quantification (right) of Annexin V positive cells in KSL fraction (*n* = 5 mice per group).
- F Levels of *Nlrp3* expression (relative quantitation, RQ) in BM-MNCs (4 months old, *n* = 6–16 mice per group).
- G, H Quantification of IL-1 β (G) and IL-23 (H) in serum (*n* = 4–12 mice per group).
- I NPM1 and P53 status in bone marrow samples of healthy volunteers, myelodysplastic syndrome (MDS), and acute myeloid leukemia (AML) with multi-lineage dysplasia (MLD) patients.
- J Schematic model of working hypothesis. *Npm1* loss causes (1) the premature aging of HSCs and (2) the activation of their mitochondria. This leads to (3) the activation of the inflammasome complex and the consequent (4) aberrant myeloid expansion. The progression of disease (5) is p53-dependent. In the *Npm1* cKO mouse model (gray), *Npm1* loss increases p53 levels that trigger apoptosis and senescence, leading to bone marrow failure. Functional loss of p53 (red, Double KO) escapes these mechanisms, feeding a positive-feedback loop between inflammation and myeloid expansion, which results in blast accumulation and leukemic transformation.

Data information: All data are shown as mean \pm SD. ANOVA test, compare each column with every column. ns or unnoted $P > 0.05$, * $P < 0.05$, ** $P < 0.01$, *** $P < 0.001$, **** $P < 0.0001$.

which leads to retention in the cytoplasm (Falini *et al*, 2005). This raises a hotly contested question: does *NPM1* mutation maintain AML through gain of function in the cytoplasm, or through reduced *NPM1* dosage in the nucleus (Heath *et al*, 2017)?

Our analysis of two cohorts of bone marrow from patients with myeloid malignancies has shown that *NPM1* expression is reduced in MDS patients (Fig 1A), and *NPM1* protein levels are low in these patients' samples (Fig 1C). *NPM1* haploinsufficiency has been observed in MDS syndromes with large 5q chromosome deletion (Berger *et al*, 2006), suggesting that this may confer a proliferative advantage in the myeloid lineage (Di Matteo *et al*, 2016). To evaluate this hypothesis, we generated a mouse model with conditional knockout in the hematopoietic compartment for the study of *Npm1* deletion *in vivo*.

Npm1 is essential for embryonic development, and its knockout has resulted in embryonic lethality between E11.5 and E12.5 (Grisendi *et al*, 2005). In this study, we utilized a new mouse line to inactivate *Npm1* through *Vav1Cre* mediation. Surprisingly our *Npm1* cKO pups were born in an expected Mendelian ratio (Fig 1E). In other research, *Npm1^{-/-}* embryos appeared pale as early as E9.5 (Grisendi *et al*, 2005) due to impairment of the blood supply from the yolk sac, suggesting that the critical period of *Npm1* expression may be earlier than E11.5, perhaps during the development of the intra-arterial clusters or endothelium. In support of this hypothesis, *VEC*-mediated inactivation of *Npm1* revealed that *Npm1* in hematopoietic cells affects early-stage embryonic development, causing a decrease in the born ratio of mice with *Npm1* loss (Fig 1G). However, regardless of the precise mechanisms involved, *Vav1Cre*-mediated inactivation of *Npm1* in the hematopoietic system has allowed us to explore its contributions to adult hematopoiesis.

Npm1 cKO mice offer a unique opportunity to explore key aspects of MDS. Perhaps first among these is aging, which represents the greatest risk factor for developing MDS. Mice harboring heterozygous loss of *Npm1* (*Npm1^{+/-}*) showed a mild MDS-like phenotype characterized by dyserythropoiesis and dysplastic megakaryocytes with macrocytic anemia, along with increased susceptibility to hematologic malignancies with age, but without significant cytopenias or alterations in lineage commitment (Grisendi *et al*, 2005; Sportoletti *et al*, 2008). We found that *Npm1* cKO mice exhibit significantly shorter survival rates compared to

Npm1 cHet mice (Fig 4A). The median survival of *Npm1* cKO mice was 353 days, but as early as 4 months, they developed MDS-like hematopoietic defects characterized by the appearance of dysplastic cells in PB smears (Fig 3F). The most peculiar feature of our *Npm1* cKO model was its phenotype in the HSC fraction (Fig 2B–H). Here, we showed that homozygous *Npm1* deletion in the hematopoietic compartment caused the expansion of a non-functional HSC pool characterized by increased frequency in CD150 positivity (Fig 2B), reduced cytoskeletal polarity (Fig 2C and D), limited *in vitro* colony replating capacity (Fig 2E), and altered mitochondria (Fig 2F–H), well-known markers of HSC aging (Morganti & Ito, 2021). These data support the idea that homozygous loss of *Npm1* causes premature aging, which makes the *Npm1* cKO a better model for the study of MDS development and progression.

We observed that *Npm1* loss caused mitochondrial alteration/activation in both murine HSCs and the MDS-L cell line, which is a human model of MDS (Fig 2F–L). Interestingly, our team has shown that the oncogenic mutant form of *Npm1* (*Npm1c*) also impairs mitochondrial function (Wu *et al*, 2021). Although a deeper investigation is needed to discover the molecular mechanisms by which *Npm1* affects mitochondrial physiology, these data suggest for the first time that *Npm1* is a regulator of mitochondrial fitness.

Mitochondrial homeostasis is crucial to control stem cell during the aging process. Mitochondrial metabolic control and ROS production regulated by SIRT3 can regulated HSC self-renewal at old stage (Brown *et al*, 2013). Another Sirtuin, SIRT7, has shown to be reduced in aged HSCs. SIRT7 mediates the mitochondrial unfolded protein response (mtUPR) pathway to alleviate mitochondrial stress, which deregulation is a contributing factor for HSC aging (Mohrin *et al*, 2015).

Mitochondrial stress can initiate aberrant activation of the NLRP3 inflammasome in HSCs, mediating their functional decline and impairing their regenerative capacity (Luo *et al*, 2019). In line with this hypothesis, we have confirmed that levels of both *Nlrp3* and its downstream target IL-1 β increased in *Npm1* cKO mice (Fig 3A and B). The related overall boost in inflammation was linked on one hand with myeloid-biased differentiation; indeed, HSCs exposed to acute IL-1 β appear to exhibit Myd88-dependent proliferation and myeloid differentiation through activation of the transcription factor PU.1 (Pietras *et al*, 2016). On the other hand, inflammation is also related to aging,

and IL-1, IL-6, and TNF levels have been found to increase two- to four-fold in old mice serum (Caiado *et al.*, 2021). Inflammatory status in turn is associated with hematological malignancies, as chronic inflammatory diseases associated with activated innate immune signaling pathways often precede MDS (Trowbridge & Starczynowski, 2021). Whether inflammation is a cause and/or a consequence of these established malignancies remains to be determined; however growing evidence has highlighted the importance of inflammatory signaling in regulating MDS progression (Sallman & List, 2019).

Myeloid-biased differentiation (Fig 3C–F) was not the only phenotype observed, and *Npm1* cKO mice exhibited significant hypocellularity in the bone marrow (Fig 4B). As previously reported (Grisendi *et al.*, 2005), *Npm1* loss evokes a p53 response, and we have confirmed that *Npm1* cKO and *NPM1*-silenced MDS-L cells express higher levels of *p53* and *p21*, which are associated with increased apoptosis, and senescence in hematopoietic progenitor cells, as well as consequent lethargic bone marrow failure (Fig 6D and E). The inflammatory cytokines enhanced in *Npm1* cKO mice (Fig 3B) can contribute to HSC exhaustion, as shown in previous reports that interferons (IFNs) can induce p53-dependent apoptosis and/or cell-cycle arrest (Pietras *et al.*, 2014), and that IL-1 can promote differentiation (Pietras *et al.*, 2016). Among the cytokines enhanced in *Npm1* cKO mice, IL-6 is of particularly high interest, since the elevated expression of IL-6 in MDS is directly linked to dysregulation of innate immune pathways. Loss of the 5q genes miR-145 and miR-146a results in TRAF6-mediated overexpression of IL-6 in HSPCs, which in turn leads to peripheral blood cytopenias and a highly penetrant bone marrow failure (Starczynowski & Karsan, 2010; Varney *et al.*, 2017).

To evaluate the contribution of p53 to disease progression, we decided to generate a double KO (*Npm1^{F/F}p53^{-/-}Vav1Cre⁺*) model (Fig EV4D). When p53 was deleted, we observed severe accumulations of the myeloid fraction in peripheral blood (Fig 4E), spleen (Fig 4H), and bone marrow (Fig 4J) at 2 months, and a reduction of overall survival to 110 days (Fig 4A). The increased levels of *p53* and *p21* observed in *Npm1* cKO indicate a cell cycle block/senescence and/or apoptotic regulation, which not only leads to defective control of HSC numbers but also suppresses aberrant myeloid progenitor cells to prevent disease progression, which was lost in our DKO mouse model (Fig 6J).

Npm1 loss generates an environment characterized by premature aging and aberrant inflammation, which predispose mice to AML progression when p53 is lost. The observations that low levels of NPM1 in MDS patients are associated with normal levels of p53, while in AML patients p53 is aberrantly expressed, support our hypothesis that *Npm1* loss generates an MDS-like phenotype which can progress to AML when p53 function is lost.

Thanks to the insights gleaned from these *Npm1* cKO and double KO mouse models, further studies, such as a detailed transcriptomic analysis, will be needed to reveal the molecular mechanisms through which inactivation of NPM1 and p53, together with aging and inflammation, are able to drive MDS and leukemia.

Materials and Methods

Patient samples

Bone marrow samples from 29 and 20 patients (Fig EV1A and B, respectively) with MDS, 49 patients with AML with multi-lineage

dysplasia (Fig EV1B) and healthy volunteers (29 and 41 samples for Fig EV1A and B, respectively) were collected between 1994 and 2010. All cases were clinically diagnosed as MDS or MLD in AML based on established criteria. Use of tissue samples was approved with an Institutional Review Board waiver and by the Human Tissue Utilization Committee.

Mice

Npm1^{F/F} mice were kindly received from Dr. Pier Paolo Pandolfi and were crossed with *Vav1Cre* transgenic mice (Jackson Laboratory) or *VE-Cadherin-Cre* transgenic mice (Jackson Laboratory). The conditional knockout allele was designed with the same strategy as the *Npm1* total-body knockout mice, where critical exons (exon 1–6) were flanked by two loxP sites (details are available in Fig 1D). Conditional deletion of these exons of the floxed *Npm1* allele in hematopoietic cells was detected by PCR (Fig EV1D). *Trp53* knockout mice and C57BL/6 mice congenic for the CD45 locus (B6-CD45.1) were purchased from The Jackson Laboratory. All mice were maintained on a C57BL/6 background and housed in microisolator cages in a pathogen-free animal facility. All procedures were approved by the Albert Einstein College of Medicine Animal Care and Use Committee.

Cell line and siRNA knockdown

MDS-L were cultured in RPMI-1640 medium, 10% Fetal Bovine Serum (FBS), 1% Penicillin-Streptomycin, 14 μ M Beta-Mercaptoethanol (Sigma) and 20 ng/ml human recombinant IL-3 (StemCell Technologies). Mycoplasma contamination test was negative. Amaxa™ Nucleofector™ II (Lonza), X-001 program and Amaxa™ Cell Line Nucleofector™ Kit T (Lonza) were used for the transfection following the manufacturer's instructions. Predesigned silencer targeting NPM1 (siNPM1) and silencer negative control (siCTRL) were obtained from Thermo Fisher Scientific (catalog number AM16708 and AM 4611, respectively) and used at 2 μ M concentration for 48 h.

Real-time RT–qPCR

Total RNA was extracted using the RNeasy Plus Mini kit (Qiagen), then reverse transcribed to cDNA with SuperScript III reverse transcription (Invitrogen) according to the manufacturer's instructions. mRNA expression levels were analyzed using TaqMan probes (Life technologies), PCR Master Mix (Thermo Fisher Scientific) and a QuantStudio 6 Real-Time PCR System.

Flow cytometry and cell sorting

Peripheral blood, spleen cells, and bone marrow mononuclear cells (BM-MNCs) were isolated as previously described (Ito *et al.*, 2016). After isolation, BM-MNCs were incubated with the following mix of monoclonal antibodies against lineage: Ly6G/Ly6C (Gr1)-biotin (108404) from Biolegend; CD11b-biotin (BDB553309), CD19-biotin (BDB553784), CD45R/B220-biotin (BDB553086), CD4-biotin (BDB553782), NK-1.1-biotin (BDB553163), and TER-119-biotin (BDB553672) from Fisher Scientific; CD135 (Flt3)-biotin (13-1351-82) from Ebioscience; CD127-biotin (13-1271-85), CD3e-biotin (13-0031-85), CD8a-biotin (13-0081-85), Mouse IgM-biotin (13-5790-85)

from Life Technologies, and then resuspended in 2% FBS-PBS for 30 min in ice. Lineage antibody staining was followed by incubation with antibody mix for the following HSPC markers: CD117 (c-Kit)-APC/Cy7 (105826), CD150 (SLAM)-PerCp/Cy5.5 (115922), CD48-Pacific Blue (103418) from Biolegend; CD48-APC (17-0481-82), Ly-6A/E (Sca-1)-PE/Cy7 (25-5981-81), Streptavidin-APC (17-4317-82) or Streptavidin-Pacific Blue (48-4317-82) from Ebioscience; resuspended in 2% FBS-PBS for 30 min in ice. All antibodies were used at a 1:100 dilution. Samples were acquired on a LSR II flow cytometer (Becton Dickinson), and then, data were analyzed using FlowJo 10 (Becton Dickinson). For cell sorting, the BM-MNCs were prepared as aforementioned, in addition cells were incubate with Anti-Biotin MicroBeads (10 μ l beads per BM, Mylteni Biotech) for 10 min at room temperature, then flow through MACS LS column (Mylteni Biotech) for lineage depletion. Cells were sorted directly into StemSPAN SFEM through a BD FACS ARIA II (Becton Dickinson). When % of another population is determined, no significant difference in the frequencies of the parent populations in BM-MNCs was confirmed, as otherwise described.

Immunofluorescence

Sorted cells were resuspended in 50 μ l of StemSPAN (StemCell Technologies) supplemented with 50 ng/ml SCF (Peprotech) and 50 ng/ml TPO (Peprotech) then seeded on Lab-Tek™ II Chamber Slide (Thermo Fisher Scientific) coated with Retronectin (Clontech). Samples were then immunostained as described previously (Bonora *et al*, 2018). Rabbit polyclonal anti-TOM20 (FL-145, Santa Cruz, dilution 1:100), anti- α Tubulin (Invitrogen, MA1-80017), and anti-CDC42 (Invitrogen, PA1092X) were used for the detection. Z-stack were acquired on a Leica SP5 equipped with 63X oil immersion lens (NA 1.4), pinhole set at 1 airy unit with voxel size 80/200 nm on XY/Z. Stacks were deconvolved using the Richardson-Lucy algorithm (Sage *et al*, 2017) using measured PSF. Representative image renderings were obtained by Imaris 7 (Bitplane).

Immunohistochemistry

Mouse tissue sections were stained with hematoxylin and eosin for histopathologic examination. Pictures of the stained tissue sections were obtained using an Olympus BX41 microscope and a DP20 camera (Olympus). NPM1 and P53 protein staining was performed using the anti-NPM1 antibody (Sigma or Dako) and anti-P53 antibody (Dako). At least 100 cells from 10 fields and 2 separated sections in each sample were counted to assess protein levels.

Peripheral blood smear and count

The collected peripheral blood was smeared for May-Grünwald-Giemsa staining (Sigma).

Briefly, the samples were stained in May-Grünwald solution for 5 min, washed in PBS for 90 s, stained in Giemsa solution for 15 min, finally washed in running tap water and let them dry. For WBC, RBC, Plt, and Hgb count an automated blood count The ADVIA® 120 Hematology system (SIEMENS) was used.

In vitro colony formation assay

Colony formation assays were performed using MethoCult (Stem Cell Technologies, Vancouver, BC, Canada) according to manufacturer's instructions. Briefly, 1500 KSL were plated per well. After 7 days the number and the nature of the colonies were estimated.

In vitro limiting dilution assay

Long-term culture assay was performed sorting 8, 4, 2, and 1 HSC (KSL CD135⁻CD150⁺CD48⁻) in single well StemSPAN SFEM (StemCell Technologies) supplemented with 50 ng/ml SCF (Peprotech), and 50 ng/ml TPO (Peprotec) for 6 weeks. Half medium was replaced once a week. Frequencies of cells with colony forming capacity after long-term in vitro culture were calculated using ELDA, extreme limiting dilution analysis (Hu & Smyth, 2009). In each experiment, 24 replicates of each dilution were performed, and L-Calctm Software (StemCell technologies) was used to investigate the difference between the two conditions.

Bone marrow transplantation

To determine the *in vivo* transplantability of the disease, 1.0×10^6 bone marrow mononuclear cells (BM-MNCs) from primary (CD45.2) moribund/deceased *Npm1* cKO, *Npm1/p53* compound mutant (DKO) mice or littermate controls (Ctrl and *p53* KO) were transplanted into irradiated recipient mice (CD45.1) with 4.0×10^5 competitor BM-MNCs (CD45.1). The transplanted mice were followed until sign of lethargy/dead and the BM of moribund/deceased transplanted mice were then analyzed.

Cytokine quantification in serum

Peripheral blood was collected from the submandibular vein of anesthetized mice. After 2 h at RT, the blood samples were centrifuged at 3,000 rpm for 5 min in order to obtain the serum fraction. The serum was transferred in a new 1.5 ml tube and used for the cytokine quantification with LEGENDplex™ Mouse Inflammation Panel (Biolegend).

Following the manufacture's instruction, the concentration of IL-1 α , IL-1 β , IL-6, IL-10, IL-12p70, IL-17A, IL-23, IL-27, MCP-1, IFN- β , IFN- γ , TNF- α , and GM-CSF were determined by interpolation from the calibration curve.

Mitochondrial membrane potential and superoxide production by flow cytometry

For mitochondrial membrane potential, freshly isolated BM stained for surface markers were incubated with 5 nM TMRM diluted in StemSPAN SFEM (StemCell Technologies) supplemented with 50 ng/ml SCF (Peprotech), 50 ng/ml TPO (Peprotec) and 50 μ M Verapamil as described in (Morganti *et al*, 2019). TMRM was incubated 60 min at 37°C. For mitochondrial superoxide, freshly isolated BM stained for surface markers were incubated with 1 μ M MitoSOX™ (Thermo Fisher) diluted in phosphate-buffered saline (PBS) supplemented with 50 μ M Verapamil. MitoSOX™ was incubated 30 min at 37°C, then washed. Samples were acquired on a LSR II

flow cytometer (Becton Dickinson), then data analyzed using FlowJo 10 (Becton Dickinson).

Apoptosis and senescence assay by flow cytometry

Freshly isolated BM stained for surface markers were stained with Annexin V apoptosis detection Kit (Biolegend) for apoptosis, and CellEvent Senescence Green Flow Cytometry Assay (Life Technologies) for detection of β -galactosidase activity according to the manufacturer's instructions. Samples were acquired on a LSR II flow cytometer (Becton Dickinson), and then, data were analyzed using FlowJo 10 (Becton Dickinson).

Statistical analysis

The sample size was chosen by the expected effect size in the individual experiments, and no statistical methods were used to ensure adequate power to detect a pre-specified effect size. The animals were randomly assigned to the individual experimental groups and the animal studies were performed under blinding condition. Statistical analysis was performed using GraphPad Prism software. All values are expressed as the mean \pm SD, unless otherwise specified in the figure legends. Unpaired two-tailed Student's *t*-tests, one-way ANOVA with Bonferroni correction, or nonparametric tests were performed, depending on the hypotheses tested, as explained in the figure legends. Results equal to or above a 95% confidence interval (*P* value \leq 0.05) were considered statistically significant. The log-rank test was used to compare mouse survival curves.

Data availability

No large primary datasets have been generated and deposited.

Expanded View for this article is available online.

Acknowledgments

We are grateful to members of the Ito lab and the Einstein Stem Cell Institute for their comments on hematology and stem cell biology, and especially thank H. Sato for her technical support, K. Gritsman for her critical reading of our manuscript, P.P. Pandolfi for the *Npm1^{F/F}* mouse strain, as well as the Einstein Flow Cytometry and Analytical Imaging core facilities (funded by National Cancer Institute grant P30 CA013330) for help carrying out the experiments. A. V. and Ke. I. are supported by grants from the National Institutes of Health (R01HL139487 and R01HL150832 to A.V., and R01HL148852, R01DK098263, R01DK115577, and R01HL069438 to K.I., respectively) and New York State Department of Health as Core Director of Einstein Single-Cell Genomics/Epigenomics (C029154). Ke.I. is a Research Scholar of the Leukemia & Lymphoma Society (#1360-19). C.M. is supported by The Einstein Training Program in Stem Cell Research, which is acknowledged from the Empire State Stem Cell Fund through New York State Department of Health Contract (C34874GC).

Author contributions

Claudia Morganti: Data curation; Formal analysis; Investigation; Writing—original draft. **Kyoko Ito:** Data curation; Formal analysis; Writing—original draft. **Chie Yanase:** Data curation; Formal analysis. **Amit Verma:** Resources.

Julie Teruya-Feldstein: Data curation; Supervision; Validation; Investigation; Visualization. **Keisuke Ito:** Conceptualization; Supervision; Funding acquisition; Investigation; Project administration; Writing—review and editing.

In addition to the CRediT author contributions listed above, the contributions in detail are:

CM and Kyl contributed to the performance of the experiments and analysis of the data. CY provided her technical support and AV shared the human cell lines. JTF provided her expertise in hematopathology. KeI conceived and directed the study. The paper was written by CM and KeI. All the authors contributed to the design of experiments, discussed the results, and commented on the manuscript.

Disclosure and competing interests statement

The authors declare that they have no conflict of interest.

References

- Asai T, Liu Y, Bae N, Nimer SD (2011) The p53 tumor suppressor protein regulates hematopoietic stem cell fate. *J Cell Physiol* 226: 2215–2221
- Berger R, Busson M, Baranger L, Helias C, Lessard M, Dastugue N, Speleman F (2006) Loss of the NPM1 gene in myeloid disorders with chromosome 5 rearrangements. *Leukemia* 20: 319–321
- Bonora M, Ito K, Morganti C, Pinton P, Ito K (2018) Membrane-potential compensation reveals mitochondrial volume expansion during HSC commitment. *Exp Hematol* 68:30–37
- Brown K, Xie S, Qiu X, Mohrin M, Shin J, Liu Y, Zhang D, Scadden DT, Chen D (2013) SIRT3 reverses aging-associated degeneration. *Cell Rep* 3: 319–327
- Caiado F, Pietras EM, Manz MG (2021) Inflammation as a regulator of hematopoietic stem cell function in disease, aging, and clonal selection. *J Exp Med* 218:e20201541
- Chambers SM, Shaw CA, Gatz C, Fisk CJ, Donehower LA, Goodell MA (2007) Aging hematopoietic stem cells decline in function and exhibit epigenetic dysregulation. *PLoS Biol* 5: e201
- Chen MJ, Yokomizo T, Zeigler BM, Dzierzak E, Speck NA (2009) Runx1 is required for the endothelial to haematopoietic cell transition but not thereafter. *Nature* 457: 887–891
- Di Matteo A, Franceschini M, Chiarella S, Rocchio S, Travaglini-Allocatelli C, Federici L (2016) Molecules that target nucleophosmin for cancer treatment: an update. *Oncotarget* 7: 44821–44840
- Falini B, Mecucci C, Tiacci E, Alcalay M, Rosati R, Pasqualucci L, La Starza R, Diverio D, Colombo E, Santucci A et al (2005) Cytoplasmic nucleophosmin in acute myelogenous leukemia with a normal karyotype. *N Engl J Med* 352: 254–266
- Florian M, Dörr K, Niebel A, Daria D, Schrezenmeier H, Rojewski M, Filippi M-D, Hasenberg A, Gunzer M, Scharffetter-Kochanek K et al (2012) Cdc42 activity regulates hematopoietic stem cell aging and rejuvenation. *Cell Stem Cell* 10: 520–530
- Giagounidis A, Haase D (2013) Morphology, cytogenetics and classification of MDS. *Best Pract Res Clin Haematol* 26: 337–353
- Goasguen JE, Bennett JM (1992) Classification and morphologic features of the myelodysplastic syndromes. *Semin Oncol* 19: 4–13
- Grisendi S, Bernardi R, Rossi M, Cheng K, Khandker L, Manova K, Pandolfi PP (2005) Role of nucleophosmin in embryonic development and tumorigenesis. *Nature* 437: 147–153
- Grisendi S, Mecucci C, Falini B, Pandolfi PP (2006) Nucleophosmin and cancer. *Nat Rev Cancer* 6: 493–505

- Heath EM, Chan SM, Minden MD, Murphy T, Shlush LI, Schimmer AD (2017) Biological and clinical consequences of NPM1 mutations in AML. *Leukemia* 31: 798–807
- Heinrichs S, Kulkarni RV, Bueso-Ramos CE, Levine RL, Loh ML, Li C, Neuberg D, Kornblau SM, Issa J-P, Gilliland DG et al (2009) Accurate detection of uniparental disomy and microdeletions by SNP array analysis in myelodysplastic syndromes with normal cytogenetics. *Leukemia* 23: 1605–1613
- Hu Y, Smyth GK (2009) ELDA: extreme limiting dilution analysis for comparing depleted and enriched populations in stem cell and other assays. *J Immunol Methods* 347: 70–78
- Ito K, Hirao A, Arai F, Takubo K, Matsuoka S, Miyamoto K, Ohmura M, Naka K, Hosokawa K, Ikeda Y et al (2006) Reactive oxygen species act through p38 MAPK to limit the lifespan of hematopoietic stem cells. *Nat Med* 12: 446–451
- Ito K, Turcotte R, Cui J, Zimmerman SE, Pinho S, Mizoguchi T, Arai F, Runnels JM, Alt C, Teruya-Feldstein J et al (2016) Self-renewal of a purified Tie2+ hematopoietic stem cell population relies on mitochondrial clearance. *Science* 354: 1156–1160
- Kida JI, Tsujioka T, Suemori SI, Okamoto S, Sakakibara K, Takahata T, Yamauchi T, Kitanaka A, Tohyama Y, Tohyama K (2018) An MDS-derived cell line and a series of its sublines serve as an in vitro model for the leukemic evolution of MDS. *Leukemia* 32: 1846–1850
- Komrokji RS, Zhang L, Bennett JM (2010) Myelodysplastic syndromes classification and risk stratification. *Hematol Oncol Clin North Am* 24: 443–457
- La Starza R, Matteucci C, Gorello P, Brandimarte L, Pierini V, Crescenzi B, Nofrini V, Rosati R, Gottardi E, Saglio G et al (2010) NPM1 deletion is associated with gross chromosomal rearrangements in leukemia. *PLoS One* 5: e12855
- Lindsley RC, Saber W, Mar BG, Redd R, Wang T, Haagenson MD, Grauman PV, Hu Z-H, Spellman SR, Lee SJ et al (2017) Prognostic Mutations in Myelodysplastic Syndrome after Stem-Cell Transplantation. *N Engl J Med* 376: 536–547
- Lopez DJ, Rodriguez JA, Banuelos S (2020) Nucleophosmin, a multifunctional nucleolar organizer with a role in DNA repair. *Biochim Biophys Acta Proteom Proteom* 1868:140532
- Lotem J, Sachs L (1993) Hematopoietic cells from mice deficient in wild-type p53 are more resistant to induction of apoptosis by some agents. *Blood* 82: 1092–1096
- Luo H, Mu WC, Karki R, Chiang HH, Mohrin M, Shin JJ, Ohkubo R, Ito K, Kanneganti TD, Chen D (2019) Mitochondrial Stress-Initiated Aberrant Activation of the NLRP3 Inflammasome Regulates the Functional Deterioration of Hematopoietic Stem Cell Aging. *Cell Rep* 26:945–954
- Matsuoka A, Tochigi A, Kishimoto M, Nakahara T, Kondo T, Tsujioka T, Tasaka T, Tohyama Y, Tohyama K (2010) Lenalidomide induces cell death in an MDS-derived cell line with deletion of chromosome 5q by inhibition of cytokinesis. *Leukemia* 24: 748–755
- Mohrin M, Shin J, Liu Y, Brown K, Luo H, Xi Y, Haynes CM, Chen D (2015) Stem cell aging. A mitochondrial UPR-mediated metabolic checkpoint regulates hematopoietic stem cell aging. *Science* 347: 1374–1377
- Morganti C, Bonora M, Ito K (2019) Improving the accuracy of flow cytometric assessment of mitochondrial membrane potential in hematopoietic stem and progenitor cells through the inhibition of efflux pumps. *J Vis Exp* 10.3791/60057
- Morganti C, Ito K (2021) Mitochondrial contributions to hematopoietic stem cell aging. *Int J Mol Sci* 22: 11117
- Morrison SJ, Wandycz AM, Akashi K, Globerson A, Weissman IL (1996) The aging of hematopoietic stem cells. *Nat Med* 2: 1011–1016
- Nagarajan L (1995) Molecular analysis of the 5q- chromosome. *Leuk Lymphoma* 17: 361–366
- Naoe T, Suzuki T, Kiyoi H, Urano T (2006) Nucleophosmin: a versatile molecule associated with hematological malignancies. *Cancer Sci* 97: 963–969
- Pang WW, Pluvinage JV, Price EA, Sridhar K, Arber DA, Greenberg PL, Schrier SL, Park CY, Weissman IL (2013) Hematopoietic stem cell and progenitor cell mechanisms in myelodysplastic syndromes. *Proc Natl Acad Sci USA* 110: 3011–3016
- Pietras EM, Lakshminarasimhan R, Techner JM, Fong S, Flach J, Binnewies M, Passegue E (2014) Re-entry into quiescence protects hematopoietic stem cells from the killing effect of chronic exposure to type I interferons. *J Exp Med* 211: 245–262
- Pietras EM, Mirantes-Barbeito C, Fong S, Loeffler D, Kovtonyuk LV, Zhang SiYi, Lakshminarasimhan R, Chin CP, Techner J-M, Will B et al (2016) Chronic interleukin-1 exposure drives haematopoietic stem cells towards precocious myeloid differentiation at the expense of self-renewal. *Nat Cell Biol* 18: 607–618
- Raval A, Kusler B, Pang WW, Weissman IL, Mitchell BS, Park CY (2012) Effect of nucleophosmin1 haploinsufficiency on hematopoietic stem cells. *Leukemia* 26: 853–855
- Sage D, Donati L, Soulez F, Fortun D, Schmit G, Seitz A, Guiet R, Vonesch C, Unser M (2017) DeconvolutionLab2: An open-source software for deconvolution microscopy. *Methods* 115: 28–41
- Sallman DA, List A (2019) The central role of inflammatory signaling in the pathogenesis of myelodysplastic syndromes. *Blood* 133: 1039–1048
- Shepherd L, Cameron C, Galbraith P, Windsor S, Lillicrap D (1991) Absence of allelic loss on chromosome 5q by RFLP analysis in preleukemia. *Leuk Res* 15: 297–303
- Shepherd PC, Bond C, Allan NC (1992) Molecular breakpoints and platelet counts in chronic myeloid leukemia. *Blood* 80: 556–557
- Sportoletti P, Grisendi S, Majid SM, Cheng K, Clohessy JG, Viale A, Teruya-Feldstein J, Pandolfi PP (2008) Npm1 is a haploinsufficient suppressor of myeloid and lymphoid malignancies in the mouse. *Blood* 111: 3859–3862
- Starczynowski DT, Karsan A (2010) Innate immune signaling in the myelodysplastic syndromes. *Hematol Oncol Clin North Am* 24: 343–359
- Swanson KV, Deng M, Ting JP (2019) The NLRP3 inflammasome: molecular activation and regulation to therapeutics. *Nat Rev Immunol* 19: 477–489
- Tefferi A, Vardiman JW (2009) Myelodysplastic syndromes. *N Engl J Med* 361: 1872–1885
- Tohyama K, Tsutani H, Ueda T, Nakamura T, Yoshida Y (1994) Establishment and characterization of a novel myeloid cell line from the bone marrow of a patient with the myelodysplastic syndrome. *Br J Haematol* 87: 235–242
- Trowbridge JJ, Starczynowski DT (2021) Innate immune pathways and inflammation in hematopoietic aging, clonal hematopoiesis, and MDS. *J Exp Med* 218: e20201544
- Varney ME, Choi K, Bolanos L, Christie S, Fang J, Grimes HL, Maciejewski JP, Inoue JI, Starczynowski DT (2017) Epistasis between TIFAB and miR-146a: neighboring genes in del(5q) myelodysplastic syndrome. *Leukemia* 31: 491–495
- Wang SA (2011) Diagnosis of myelodysplastic syndromes in cytopenic patients. *Hematol Oncol Clin North Am* 25: 1085–1110
- Wu H-C, Rérolle D, Berthier C, Hleihel R, Sakamoto T, Quentin S, Benhenda S, Morganti C, Wu C, Conte L et al (2021) Actinomycin D targets NPM1c-primed mitochondria to restore PML-driven senescence in AML therapy. *Cancer Discov* 11: 3198–3213